Influences of Pre-treatment Steps and Contaminants in a Pyrometallurgical Recycling Process for NCA ($LiNi_{0.8}Co_{0.15}Al_{0.05}O_2$) Lithium-Ion Battery Material

L. Wiszniewski,* C. Gatschlhofer, A. Krammer, T. Hochsteiner, A. Holzer, H. Raupenstrauch

Chair of Thermal Processing Technology, Montanuniversitaet Leoben, Leoben, Austria

**Correspondence: lukas.wiszniewski@unileoben.ac.at; Tel.: +43-3842-402-5819*

The rising demand for lithium-ion batteries, coupled with international climate targets, emphasises the need for circular economy and zero-waste recycling approaches. However, so far, no industrial-scaled solutions are available that fulfil global recovery targets. Therefore, a novel pyrometallurgical reactor was developed at the Chair of Thermal Processing Technology at Montanuniversitaet Leoben to avoid lithium slagging and recover volatile elements via the gas phase. Nevertheless, previous results show that several impact factors, including interfering elements or pre-treatment steps, strongly limit the recycling efficiency of black mass. To simulate the black mass and provide feedback on possible influences of pre-treatment steps, cathode material from production with additives of interfering elements was analysed regarding melting behaviour. The results show that formation of a further processable alloy was increased by almost 50% when pre-treatment steps were excluded, indicating pre-treatment steps as a major influence to be considered within this specific recycling route.

INTRODUCTION

To counteract global warming and achieve political independence for resources like oil and gas, several emission-intensive sectors must be introduced with alternative technologies. In particular, industries with high energy demand, like the iron and steel industry (Nurdiawati and Urban, 2021), the electricity grid (Lamnatou et al., 2022), and the mobility sector (Nguyen et al., 2021) have seen major efforts for a rapid transition towards clean technologies in recent years. An important measure to reach international climate targets is the electrification of these sectors, offering the possibility to introduce renewable energies for modern societies (Teske et al., 2021). However, to avoid collapses of the electrical grid caused by fluctuating energy consumption and energy conversion of renewables, in addition to meeting an exponential increase in demand for electric vehicles around the globe, battery technologies, including a suitable recycling process, are required.

For 2030, a total capacity of up to 2600 GWh of batteries is expected, representing a 14x increase in today's installed capacity (Global Battery Alliance). Approximately 82% of this market growth will come from lithium-ion batteries (LIB), mainly caused by the almost exponential growth of demand within the mobility sector (Zhao et al., 2021). While the mobility sector has unique requirements for battery systems, other sectors rely on different battery characteristics. By adjusting the chemistry of the cathode material, these specific requirements can be fulfilled (Xu et al., 2020). Although a major milestone in battery development has been achieved with the increase in knowledge of the electrochemical behaviour of various cathode chemistries, the fluctuating recycling stream still creates significant problems at the end of life of a battery system. Within the idea of a circular economy, developing efficient recycling

Copper Cobalt Africa 2023 Conference
13–15 June 2023, Avani Victoria Falls Resort, Livingstone, Zambia
The Southern African Institute of Mining and Metallurgy

technologies for battery systems, which are energy efficient and insensitive towards a fluctuating input stream, is of utmost importance. With Directive 2006/66/EC and its revised version No. 2019/1020, the European Union stipulates specific recovery rates within recycling chains for LIB to avoid shortcuts in material availability and achieve political independence. According to a revision proposal of this directive, mandatory recovery rates of 95% for Co, Cu, and Ni, and 70% for Li should be implemented by 2030 (European Commission). Neither hydro- nor pyrometallurgical processes are yet available to fulfil these targets. Pyrometallurgical processes need large amounts of energy in form of fossil fuels and face the bottleneck of lithium slagging (Gerold et al., 2022). Hydrometallurgical methods are sensitive towards varying input streams and have to use large amounts of harsh chemicals (Sojka et al,. 2020).

Nevertheless, the first step of battery recycling, independent of the further process, is the pre-treatment. Hydrometallurgical techniques rely on an effective pulping process and a homogeneous input stream, as each metallic impurity adds one to two additional process operations (Vest, 2016). Although pyrometallurgical methods are less sensitive to changes in the input stream composition, Holzer et al. (2023) found that a specific amount of impurities can negatively affect the melting behaviour of the active material (AM) and therefore downgrade the overall process of the unique reactor concept also researched in this work. Pre-treatment of the batteries therefore plays a crucial role in the downstream treatment. Figure 1 depicts typical pre-treatment steps, starting with sorting by size and shape, commonly done manually, and discharging to reduce self-ignition risk. This deactivation can be done by short-circuiting, heating, or cooling, and using an aqueous solution (Yu et al., 2021). After dismantling, the batteries can be treated by a series of techniques to reduce the particle size, like crushing, milling, shearing, and tearing, followed by sieving and classification (Kim et al., 2021). The collector foils, consisting of Cu and Al, are more ductile compared with the AM, so they tend to stay in coarser fractions, while the electrode materials can be found in finer particle size fractions (Liu et al., 2020; Zhang et al., 2014; Or et al., 2020). However, due to larger openings in industrial screens to increase the output, a higher portion of the collector material, up to 20 mass% of the initial Cu and Al, ends up in the black mass, which mainly represents the finer fractions (Ruismäki et al., 2020). The particles subsequently undergo further physical separation methods, such as magnetic separation and flotation, to concentrate the valuable metals. As a last step, the organic binder, such as polyvinylidene fluoride (PVDF), has to be removed either by thermal treatment or a dissolution process (Kim et al., 2021). After the pre-treatment processes, metal recovery from the black mass of spent LIB can be conducted via hydro-, pyro-, or biometallurgy, and/or combined processes. A vital function of the pre-treatment is also limiting the carbon content in the black mass, which originates from the anode material and the PVDF binder (Natarajan et al., 2018). The graphite can either be recovered by flotation, as it has a good floatability in contrast to cathode material, or by a thermal treatment (Yu et al., 2021).

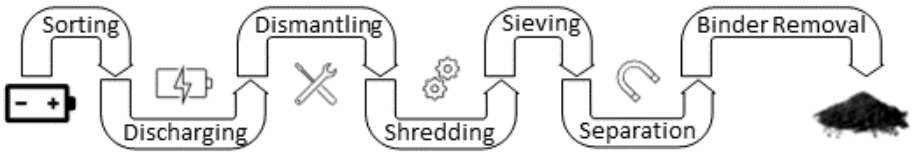

Figure 1: Simplified depiction of a common pre-treatment process (Kim et al., 2021; Yu et al., 2021).

Holzer et al. (2022a, 2023) found that a surplus of carbon above the stoichiometric demand negatively affects the melting ability in specific recycling routes. This refers to Al's functions as a potent reducing agent. Another factor, concerning hydro- and pyrometallurgy, is that black mass with a high carbon content, which is often not economically recyclable, increases the input stream and therefore lowers the efficiency of the whole process.
Pre-treatment steps show influences on both pyro- and hydrometallurgical processes and must be considered in a holistic recycling approach. Furthermore, impurities like Al, Cu, and C can impact the smelting behaviour in pyrometallurgical processes, which can also affect the gasification of Li and P in the reactor concept described below. In contrast, it was shown that, in hydrometallurgy, impurities increase the operational efforts and, therefore, the overall efficiency.

An innovative pyrometallurgical recycling concept was developed at Montanuniversitaet Leoben to

avoid the aforementioned challenges and to play a crucial role in achieving the amended recovery targets. This reactor principle offers very homogenous thermal conditions, the use of renewable energies, and the possibility to extract Li and P via the gas phase (Ponak, 2019; Windisch-Kern et al., 2021b; Holzer et al., 2022b). In recent studies and projects, theoretical and practical basic research activities have led to a profound data basis of thermochemical behaviour of LIB AM under reducing conditions (Windisch-Kern et al., 2021a, 2021b; Holzer et al., 2022b.). Although good melting ability and recovery rates for all crucial metals were achieved for trials with pure cathode materials, first trials with black mass from spent LIB showed that either interfering elements, like Cu or Al, or pre-treatment steps, like flotation, negatively influence the melting behaviour (Holzer et al., 2023). Therefore, this paper focused on comparing pyrometallurgical recycling efficiencies between LIB black mass and cathode material from production with interfering elements within a holistic and novel approach of LIB AM recycling. In view of a direct reuse possibility, interfering elements are characterised as elements occurring in any phase of the products of the pyrometallurgical process that are not part of the original cathode material. Results obtained from Holzer et al. (2023), in which a combined hydromechanical and pyrometallurgical recycling approach for LIB AM was investigated, were compared with modified cathode material from production with different concentrations of interfering elements such as C, Fe, Cu, and Al. The goal was to obtain almost the same chemical composition (related to the elements with the largest mass%) as within the AM. This comparison should provide information about possible influences of pre-treatment steps conducted in Holzer et al. (2023).

EXPERIMENTAL

Material

Pure lithium-nickel-cobalt-aluminium-oxide (NCA chemistry, $LiNi_{0.8}Co_{0.15}Al_{0.05}O_2$) cathode material from LIB production (Gelon Energy Corp., Linyi, China) was used as base material for the pyrometallurgical tests. Additional C was added as a reducing agent, and Al, Cu and Fe to simulate undesired accompanying elements.

The source material of Holzer et al. (2023) was black mass of pre-treated NCA-cells (Panasonic NCR 18650A – $LiNi_{0.8}Co_{0.15}Al_{0.05}O_2$) provided by Fraunhofer IWKS, Hanau, Germany. Black mass or AM is a fine black powder consisting primarily of cathode material with residues of Al, Cu, Fe, and C. Al and Cu originate from the electrode conductor foils, Fe is part of the casings of the batteries, and C comes from the anode material. Furthermore, black mass contains additional elements not further considered within this paper due to their negligible concentrations.

To provide comparability between both trials, the same pyrometallurgical setup was applied for the reduction processes and further metal recovery. Detailed pre-treatment steps fot the LIB AM are specified by Holzer et al. (2023). Table 1 shows the chemical compositions of the NCA_C samples, evaluated via HSC-Chemistry® and inductively coupled plasma optical emission spectroscopy (ICP-OES), and of the AM, analysed via ICP-OES.

Table 1. Chemical composition of input materials, mass%.

Sample	Li	Co	Ni	Al	Fe	Cu	C
NCA_C	4.99	6.36	33.77	2.85	3.43	6.36	19.23
NCA_AM*	3.48	5.07	30.70	1.88	3.43	6.36	19.23

*Data taken from Holzer et al. (2023)

The proportion of O, elements with lower concentration, or measurement uncertainties can explain deviations from 100% detection rate. Cathode material (NCA_C) for the synthetic replica and AM (NCA_AM) for the black mass from Holzer et al. (2023) are used as denotations in the following work.

Pyrometallurgical Treatment

At the Chair of Thermal Processing Technology at Montanuniversitaet Leoben, a novel reactor, initially developed to recover P from sewage sludge ashes, provides characteristics to avoid problems within state-of-the-art pyrometallurgical LIB recycling approaches. With the core principles of the InduRed

reactor (Figure 2a), the InduMelt plant (Figure 2(b)) has shown a huge potential to recover not only critical elements such as Co, Ni, or Mn in the form of an alloy, but also volatile elements, such as Li or P, via the gas phase.

Within the InduRed reactor, material is continuously fed from above, melts, and builds a thin molten film towards the bottom of the reactor. Inductive heating of the graphite cubes offers a homogenous radial temperature distribution, making the process strongly consistent. The graphite cubes mainly act as susceptor material because additional carbon is added as a reducing agent, avoiding wear of the graphite cubes. This enables a high surface and contact area between graphite cubes and input material, offering the possibility for short diffusion paths for volatile elements like Li or P through the melt film. Instead of being slagged or integrated into the metal phase, these volatile elements are extracted via the gas phase and can be transferred into a secondary processing and refinement step. In the case of carbon oxidation, the excess supply of reductant reduces the partial pressure of CO_2 in the reactor interior due to the Boudouard equilibrium. Therefore, ideal reduction conditions can be guaranteed in terms of low O_2 partial pressure and a high CO/CO_2 ratio. Furthermore, with renewable energies as a power supply and the replacement of the bulk material with biochar, the plant design has the potential to reduce the overall environmental impact of the LIB life cycle drastically.

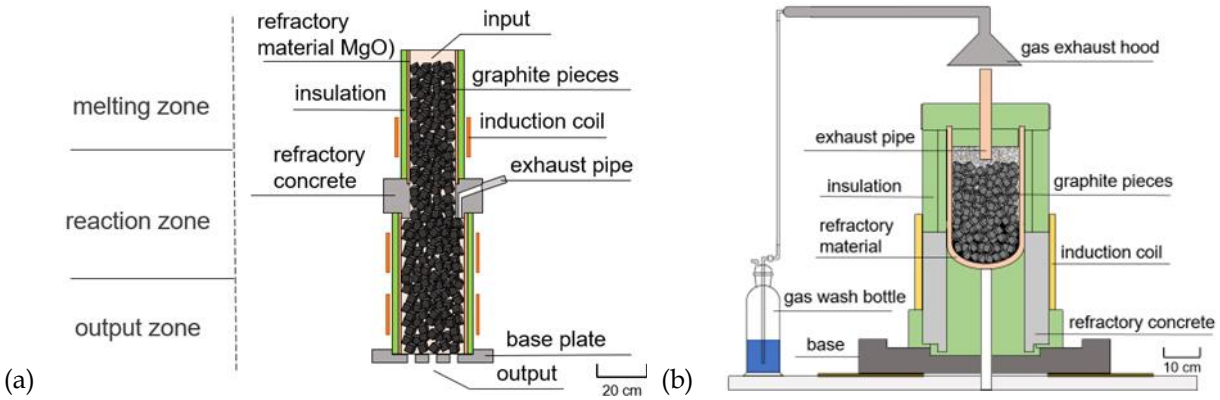

Figure 2: Schematic illustration of a) described pyrometallurgical principle within InduRed reactor (Holzer et al., 2022a) and b) InduMelt plant (Holzer et al., 2023).

To shorten individual melting trials, a laboratory-scale version of the InduRed reactor, the so-called InduMelt plant, was developed. As described in Holzer et al. (2022b), the same setup and experimental procedure were applied to achieve comparable results with previous test series. Summarised, the InduMelt plant consists of a cylindrical MgO crucible with a domed bottom, a height of 60 cm, and a diameter of 20 cm. The reactor is filled with layers of 10–15 cubes, with a third of the feedstock to be melted, added between each layer. The graphite cubes have a side length of approximately 24.5 ± 1.5 mm, an electrical resistance of 4–8 μΩ·m, and a density of 1.55–1.75 g·cm^{-1}. Owing to thermomechanical limitations of the refractory material, the heating rate was restricted to a maximum of 250°C/h until reaching a maximum temperature of about 1550°C. The temperature was monitored by three type K thermocouples, located inside the reactor, one at the height of each layer. Moreover, two type S thermocouples were placed outside the crucible surface in the middle of the cylindrical part and the middle of the domed bottom part. The crucible was insulated, as seen in Figure 2(b) (green colour), with refractory mats consisting mainly of SiO_2 and Al_2O_3. To enable the discharge of exhaust gases, a ceramic pipe was placed in the lid insulation. A gas extraction hood was placed above the ceramic pipe to convey the exhaust gas into the downstream gas-washing bottle. For this experiment, distilled water was used, preventing any undesired reactions between the fluid and the compounds in the gas stream. The heating phase lasted approximately 8 h and was followed by a holding time of about 30 min at maximum temperature. The crucible within the refractory material, including the insulation mat, was then cooled for approximately 24 h at room temperature. Within the standardised sampling method described in Holzer et al. (2022b), the resulting fractions (metal, magnetic powder, sparse-magnetic powder) were manually sieved to a generated grain size under 1 mm and separated via a neodymium bar magnet. Representative samples were further analysed with following methods.

Analytical Methods for Material Characterisation

For the evaluation of the elemental composition of the obtained fractions and recovery extents, all fractions, including the washing water, were analysed via ICP-OES according to ÖNORM EN ISO 11885:200911 in the first step. Analysis of adhesions occurring from the gas stream within the gas extraction hood and on the surface of the upper graphite cubes was carried out by laser-induced breakdown spectroscopy (LIBS; model EA-300, Keyence [optics 300x, laser–Nd: YAG 355 nm]). X-ray diffraction (XRD) supported the analysis. XRD measurements were performed using a powder X-ray diffractometer (Bruker D8 Advance ECO) in Bragg-Brentano geometry with Cu Kα radiation (λ = 0.15418 nm) at 25 mA and 40 kV. Diffraction patterns were collected in the 2θ range from 10° to 100° with a step size of 0.02° and 2 s acquisition time per step. XRD patterns were analysed using the SIeve+ software with PDF-4+ 2022 database (ICDD, USA).

The metal fractions were embedded in an epoxy resin as a polished specimen sputtered with gold and analysed via scanning electron microscope (SEM; Vega1, Tescan, Czech Republic), whereby energy-dispersive X-ray analysis (EDX; model 5108, Oxford Instruments, Si(Li) type) software largely corrected the gold signal. These assessments were executed with a variable acceleration voltage range of 0.5 – 30 kV, emanating from an electron source in the form of a tungsten filament. Furthermore, the samples were assayed by EDX, which enabled the identification of the elemental composition within a 10 mm^2 area of the sample, with a resolution of 137 eV at an acceleration voltage of 5.9 kV.

The tools and techniques presented in this study offer a comprehensive and holistic approach towards the characterisation of substance flow, enabling qualitative and quantitative assessments. These methods serve as the foundation for understanding potential reaction mechanisms and form the basis for subsequent investigations.

RESULTS AND DISCUSSION

In Holzer et al. (2023), a novel process chain approach comprising pyrometallurgical reduction combined with upstream pre-processing steps of black mass was introduced. Therein, unwanted impurities such as Al and Cu should be separated from the AM in a first hydromechanical pre-treatment. For this reason, the source material, discharged end-of-life NCA cells of an e-bike, were exposed to shock waves. Analysis results confirmed that no change in the NCA microstructure could be observed. Furthermore, NCA particles were successfully separated from the electrode foils, whereas minor amounts of Cu and Al were still found in the feed for the InduMelt plant. While the former potentially improves the melting ability, Al adversely influences the formation of a molten bath. Then, by flotation, the carbon content is set to a desired target value, providing the stoichiometrically required amount of reducing agent for carbothermal reduction. The carbon content could be diminished to 19.23 mass%, roughly representing the calculated stoichiometric demand of the reductant. After pyrometallurgical treatment, no Li could be found in the Ni-Co-Cu rich alloy, while minor amounts were identified in the mineral caking on the metal particles. However, Li preferably accumulated in the region of grain boundaries between metallic and mineral phases. Li_2CO_3 and LiF were discovered in deposits inside the off-gas line and washing water. A significantly higher ratio of powder to metal compared with experiments with pure cathode material emphasised the urgency for understanding impurity behaviour during carbothermal treatment and their impact on the output material quality. Thus, many melting experiments in a heating microscope were carried out. Different variations of the input composition, especially for the elements Cu, Al, and C, were tested and expressed in a contour diagram. The criterion used for this purpose was the change in the cross-sectional area during the heating microscope tests. From there, limiting concentration ranges in which the formation of a melt is favoured were defined. In general, for an efficient carbothermal reduction in a bulk of graphite pieces, future black mass modification should guarantee a liquid state of all formed phases. Moreover, lithium slagging or its incorporation into the metal or mineral phase should be kept to a minimum. This work aimed to replicate the pre-treated black mass of Holzer et al. (2023) using synthetically produced material. Mixtures with and without iron as an interfering element were treated in the InduMelt at 1550°C. Results presented characterise the obtained fractions after carbothermal reduction, supported by analysis methods given above, whereby a comparison is drawn with the work of Holzer et al. (2023).

Pyrometallurgical Treatment

Cathode material from battery production mixed with high-purity chemicals was used to examine the permissibility of replicating NCA-black mass as within Holzer et al. (2023). NCA cathode material with the elemental composition depicted in Table 2 was used as input material. Interfering elements were added afterwards to obtain the chemistry described in Table 1. Deviation from 100% detection rate can be explained by the proportion of O, which cannot be detected by ICP-OES, and measurement uncertainties.

Table 2. Chemical composition of NCA cathode material, mass%.

Compound	Li	Ni	Co	Al
NCA	7.38	56.1	5.34	0.92

The mixture was subsequently exposed to reducing conditions in the InduMelt's inductively heated packed bed at a maximum temperature of 1550°C. Gained fractions from the experimental setup were divided concerning characteristic material properties as follows:

- Strongly magnetic metal alloy;
- Powder: Magnetic and sparse magnetic (fractions with grain size < 1 mm);
- Deposits from the exhaust hood;
- Dissolved species in the gas wash bottle.

While the latter two fractions mentioned could be assigned to the gas line, the first three were isolated from the reactor interior. The obtained quantities are summarised in Table 3.

Table 3. Mass fractions of input and output materials of InduMelt experiments, g.

Sample	Input	Metal	Powder magnetic	Powder sparse-magnetic
NCA_C	400	181.4	46.1	2.2
NCA_AM*	400	92.5	123.0	2.7

*Data taken from Holzer et al. (2023).

Compared with Holzer et al. (2023), about twice the amount of metal alloy was recovered. In addition, significantly lower amounts of magnetic powder (46.1 g for NCA_C) resulted compared to pyrometallurgical treatment of black mass (123.0 g). This deviating trend could either be attributed to reactivity differences of the present reducing agent, a potential chemical change within the NCA cells over the life cycle of the e-bike, or structural changes within pre-treatment steps. In general, it can be summarised, that changes in the structure and chemical composition impair the reduction process, resulting in a higher ratio of undesired powder. However, the strong magnetic properties of the powder fraction can be due to therein distributed tiny reduced or partly reduced metal droplets. Therefore, a higher actual amount of recovered metal can be presumed. The fraction of sparse-magnetic powder, with its minor amounts of 2.2 g for NCA_C, are not part of further considerations for this work. The obtained fractions after the InduMelt trials are shown in Figure 3.

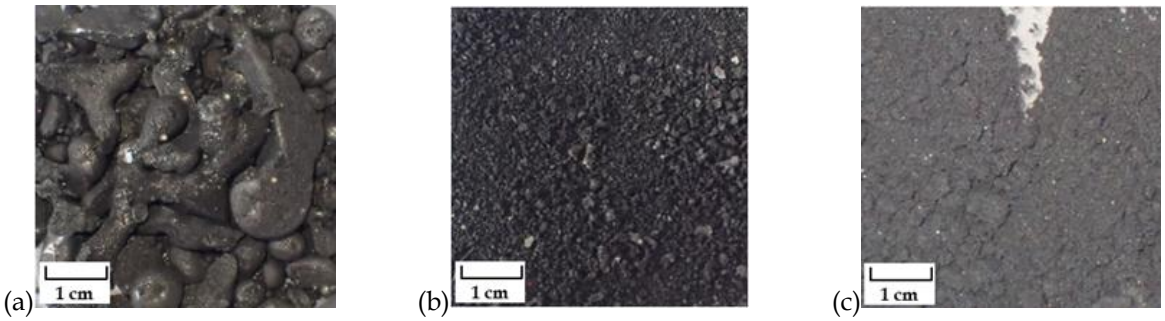

Figure 3: Obtained fractions after InduMelt trial. (a) Metal, (b) powder magnetic, (c) powder sparse-magnetic.

The output mass of NCA_C consisted of 79 mass% metal, 20 mass% magnetic powder, and about 1 mass% sparse-magnetic powder. Nonetheless, the powder content must be reduced to zero, since the formation of a molten phase is required for a continuously operated process; otherwise, in the worst

case, the powder can lead to clogging of the reactor.

Analysis of metal fraction

As seen in Table 3, metal is the predominantly generated fraction after high-temperature treatment of the NCA_C sample. Moreover, it accounts for the most significant monetary share of each fraction obtained. Consequently, the alloy is of enormous value in terms of productivity. In addition to determining the elemental composition by ICP-OES (table 4), the metal fraction was also analysed by SEM-EDX, identifying the element's contribution and allocation to the metal phases formed. Owing to the high reactivity of Al, a more potent reducing agent than C, it can be assumed that it will be in an oxidic state after the reaction process. Hence, its content can be explained by adhesions of mineral origin at the metal particle's surface. However, a relatively high ratio of Li can be found in the metal for the NCA_C sample. As described later, removing gaseous products was insufficient, resulting in unwanted long retention times of Li in the reactor interior and therefore longer contact time between Li and the solid phases. Summed values above and below 100 mass% may result from measurement inaccuracies or unmeasured elements that are not considered due to low mass percentages.

Table 4. ICP-OES analysis of different metal fractions after InduMelt experiment, mass%

Sample	Li	Co	Ni	Al	Fe	Cu
NCA_C	0.52	7.48	68.70	1.82	7.49	12.60
NCA_AM*	0.00	12.60	63.80	2.86	7.50	14.30

* Data taken from Holzer et al. (2023).

The elemental distributions of various elements in the metal alloy of sample NCA_C are shown in Figure 4, provided by mapping with SEM-EDX. Supported by the results of ICP-OES, it can be stated that the studied metal particles were rich in Ni with other typical alloying elements such as Cu, Co, and Fe. In addition, the metal particles were interspersed with elongated graphite crystallites. For clarification, the high C signal around the metal particle stems from the resin and is not considered part of the metal fraction. Neither higher quantities of oxygen nor aluminium were detected, thereby confirming favourable reduction conditions.

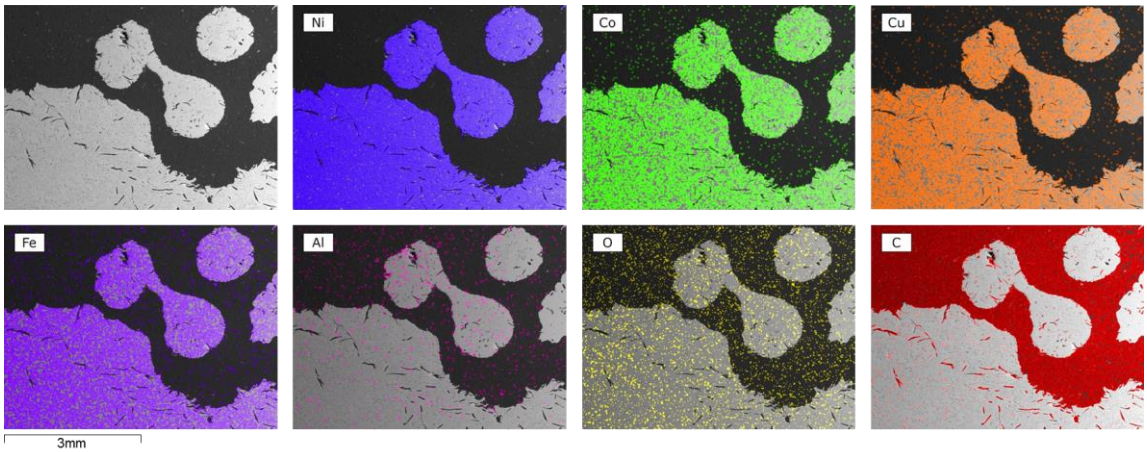

Figure 4: SEM pictures of metallic fraction and overlay of elemental distribution of characteristic elements.

To specify the mapping results, a total of seventeen points were examined through identical metal particles with a line spectrum, illustrated in Figure 5. The metal alloy was generally uniformly composed, with the upper metal particle (spectra 2–6) slightly enriched in Al compared to the lower metal particle (spectra 8–17). In some places (spectra 8, 16, and 17) no C could be measured, whereby C was detected in the remaining points of the alloy. In addition, gold was sputtered onto the metal surface during sample preparation, so a signal for gold was received on all spectra. Owing to the low element detection, it should be mentioned that only a qualitative statement about the proportion of the individual elements can be made with a line spectrum. However, the compositions are in good agreement with ICP--OES, while Li cannot be determined with this method.

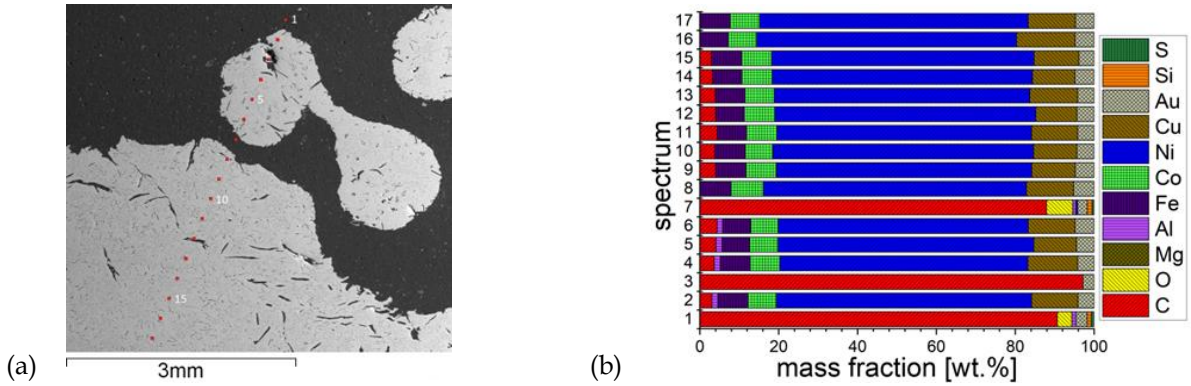

Figure 5: Line spectrum across the analysed metallic fraction. (a) SEM picture with the corresponding analysis points; (b) related composition of each point from Figure 4(a), analysed via EDX.

Analysis of powder fractions

Results from Holzer et al. (2023) showed that the proportion of powder for use in an industrially operated process is too large and must be significantly reduced to enable economical operation. The essential question of whether the influence of interfering elements, or possible influences from pre-treatment steps, such as agglomeration, was the main reason for the low formation of the metal phase, can be answered with the help of the ICP measurements and sampling results. As seen in Table 3, the proportion of powder within the trials with cathode material from production was significantly lower compared with tests with the AM. However, the chemical composition was relatively constant between all tests for both the magnetic and sparse-magnetic powder, as seen in Table 5. The description of the powder samples is abbreviated as follows: NCA_C_SMP is the sparse-magnetic powder fraction of sample NCA_C, and NCA_C_MP is the magnetic powder fraction of sample NCA_C. The same abbreviation rules belong to the sample NCA_AM.

Table 5. ICP-OES analysis of different powder fractions after InduMelt experiment, mass%.

Sample	Li	Co	Ni	Al	Fe	Cu
NCA_C2_SMP	11.70	0.05	0.59	10.70	0.08	0.10
NCA_C2_MP	3.38	4.28	36.70	9.35	4.48	7.58
NCA_AM_SMP*	5.33	0.18	7.29	2.89	0.18	0.23
NCA_AM_MP*	0.23	9.63	56.60	2.66	5.37	11.10

* Data taken from Holzer et al. (2023).

The results of the ICP-OES measurements show that the contents of Cu, Fe, Co, and Ni tended to have values in a similar range. In contrast, the contents of Al and Li were much higher within the trials of cathode material from production than the results of the AM. The higher content of Al is described in Figures 4 and 5, which show much lower concentrations of Al in the metal phase compared to the results within Holzer et al. (2023). Additionally, the proportion of powder in both trials with cathode material is reduced by more than 50%, which leads to an enrichment of base metals such as Al in the powder fraction. Since Li shows a high tendency to be slagged when it gets in contact with Al, the high proportion of Li in the powder fraction NCA_C can also be explained by the high contents of Al in this sample (Sommerfeld et al., 2020). Additionally, the content of Li was about 50% higher in the sample NCA_C compared with the AM, which might lead to a higher partial pressure of evaporated Li and, therefore, stronger integration of Li in the powder fraction. Although the amount of powder could have been significantly lowered, further investigations must be done to decrease it to a minimum.

Analysis of gaseous fractions

Several products of the gaseous fractions were analysed to understand and validate previously assumed reactions of Li at high temperatures and under reducing conditions. High amounts of white residues were found on the surface of the highest-situated graphite cubes in the reactor, which led to the conclusion that the degassing did not function optimally. These precipitates within the NCA_C trial are shown in Figure 6 and are also a possible solution for the high amount of Li in the powder fractions.

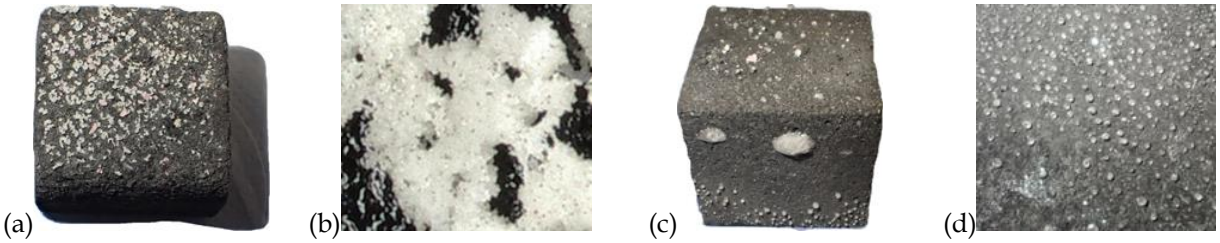

Figure 6: Precipitates on the surface of the graphite cubes. (a) Cube from the upper layer with Li_2CO_3 flakes; (b) LIBS digital image of flakes from Figure 6(a); (c) cube from middle layer with smaller and bigger crystallites; (d) high-resolution image of smaller crystallites from Figure 6(c).

A LIBS analysis was taken in the first step to validate occurring phases, followed by the powder XRD (PXRD) scan depicted in Figure 7. The PXRD scan confirmed with high probability a Li_2Co_3 phase in the diffraction pattern. Additional reflections indicate the presence of carbon and a compound with a rock salt-type structure. Reflection positions of the latter are consistent with $Li_{0.14}Co_{0.86}O$, a Li-doped CoO, which forms at high temperatures in reducing conditions, but might also be due to MgO, used as crucible material, which has the same reflection positions (Johnston et al., 1958). Further investigations regarding the CoO have to be done, to fully verify the existence and building of this phase.

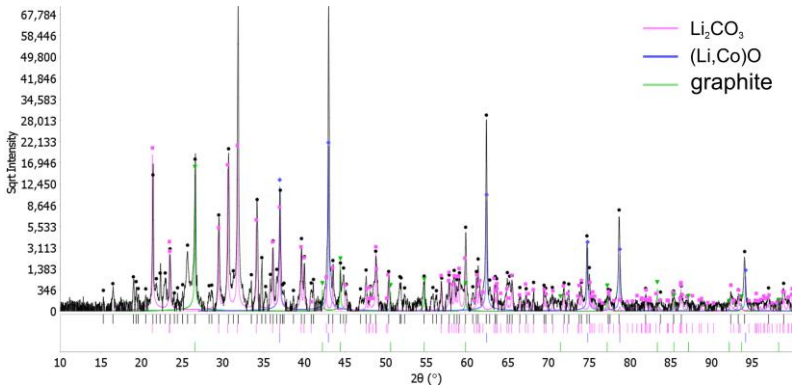

Figure 7: PXRD pattern of adhesion of a precipitate from the gas phase to the graphite cubes surface.

The residues on the graphite cube surfaces were then investigated. Precipitates in the extraction hood were mechanically removed and analysed with the same procedure. Figure 8 shows LIBS analyses of the white powder from the gas extraction hood.

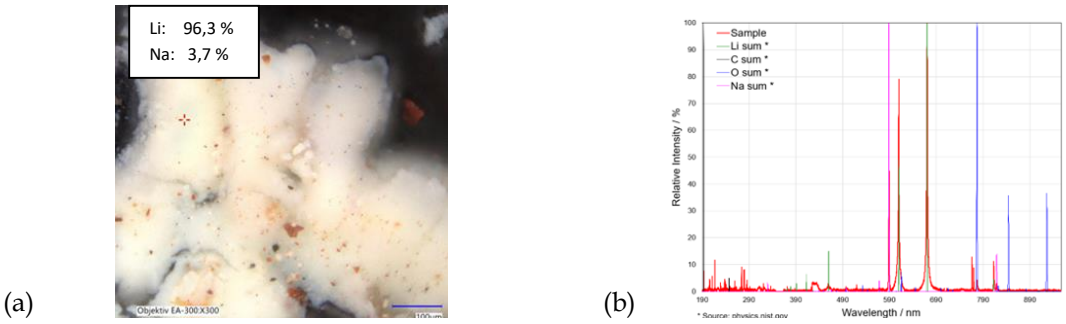

Figure 8: LIBS analysis of accumulations of gaseous precipitation in extraction hood. (a) Digital microscopic image with analysis point in red; (b) corresponding LIBS pattern with characteristic elemental peaks

As described in Windisch-Kern et al. (2021b) and Kwon and Sohn (2020), the thermal stability of lithium metal oxides ($LiMeO_2$) can be lowered when a reductant like C is added. Additionally, the formation of Li_2CO_3, as described in Equation 1, is favoured, compared with the formation of lithium oxide without a reductant. However, at higher temperatures, the decomposition of Li_2CO_3 to Li_2C_2 is likely to occur, further decomposing in gaseous Li (Holzer et al. 2022b). Complementary analyses via simultaneous

thermal analysis are planned to predict the exact reaction mechanism.

$$4\ LiMeO_2(s) + 3\ C(s) \rightarrow 2\ Li_2CO_3(s) + 4\ MeO(s) + CO_2(g) \quad [1]$$

The water of the gas wash bottle and resulting filtrate, a white powder, were also analysed via ICP-OES to understand the chemical composition and possible gasification rates. As seen in Table 6, the trial with AM showed much higher concentrations of Li than the experiments of the cathode material from production. In NCA_C, the Li concentration was extremely low, which might result from the mechanical removal of the white residue from the gas extraction hood. The gaseous samples are abbreviated as follows: NCA_C_W is the composition of the washing water of sample NCA_C. The same abbreviation rules belong to the sample NCA_AM.

Table 6. ICP-OES analysis of washing water samples after InduMelt experiments, mg/L.

Sample	Li	Co	Ni	Al	Fe	Cu
NCA_C2_W	160.0	0.0	0.5	0.0	0.0	0.7
NCA_AM_W*	640.0	0.0	2.5	0.7	0.0	9.0

* Data taken from Holzer et al. (2023).

Although improvements regarding Li extraction can be performed, the analysis results showed that 89.7% of the Li from the input feed was not found and therefore either removed via the gas phase or discovered as white precipitates on the graphite cubes surfaces.

CONCLUSION

In the presented work a comparison regarding recycling efficiencies between LIB black mass and cathode material from production with interfering elements, simulating a synthetic black mass, was conducted within experimental trials. To provide the same elemental composition as the black mass analysed in Holzer et al. (2023), NCA cathode material from production was blended with pure substances, representing interfering elements such as C, Cu, Al, and Fe. The goal of this comparison was to analyse whether these interfering elements, or pre-treatment steps like flotation, led to poorer melting abilities. Despite a similar chemical composition of the input material (LIB black mass vs. synthetic black mass) and obtained fractions after carbothermal treatment, the latter proportions showed a strong deviation. For instance, with synthetic black mass, approximately twice the amount of a metal alloy was generated. SEM-EDX analysis confirmed a high Ni content, with significant amounts of Cu, Co, and Fe. In contrast, the proportion of powder was reduced by more than half. Results from the analysis clearly indicate that the reason for the reduced melting behaviour was not due to the presence of possible interfering elements, but more likely can be explained by structural changes in the black mass during the LIB utilisation phase or pre-treatment steps of the black mass. Although the ratio of a metallic fraction within the test of the synthetic black mass was high, the undesired powder was still present and, therefore, could not be transferred into a molten state.

The goal to reduce the powder content was achieved, so the share of Li within the solid fractions gained from the reactor interior was more than double that in the solid fractions of Holzer et al. (2023). As the formation of a molten phase is essential for the functionality of the reactor, further investigations must be undertaken to maximise the metal output. These include determination of the required reducing agent amount. Owing to the additional presence of Al, a stoichiometric amount of C could be too high, impairing the meltability of the input mixture. High contents of Li in the solid phases and high Li amounts bound as lithium carbonate deposits on the graphite cube surfaces could be attributed to an inadequate discharge of gaseous products from the reactor interior. Therefore, the reactor design, in particular the lid and associated gas vent, must be revised. In addition, sampling of the obtained fractions must be reconsidered. The preparation itself, where solid phases with a grain size smaller than 1 mm were counted as part of the powder fraction, could still contain a high proportion of smaller metal particles. This assumption is confirmed by the results of ICP-OES and proof of magnetic properties, indicating the presence of metallic droplets. However, the identification of possible causes for the

deviation between high-temperature treatment of black mass and synthetic black mass should be focus of future research efforts in this field. Furthermore, it is imperative to identify other factors that exert an influence on the AM's structural modifications during the lifespan of an LIB.

ACKNOWLEDGEMENTS

Great thanks are owed to Simon Moll and Elias Vigl for supporting with SEM-EDX and LIBS analyses, to Daniel Schrittwieser for preparation of the SEM samples and to Andreas Egger for the PXRD scans. The project FuLIBatteR is supported by COMET (Competence Center for Excellent Technologies), the Austrian programme for competence centers. COMET is funded by the Federal Ministry for Climate Action, Environment, Energy, Mobility, Innovation and Technology, the Federal Ministry for Labour and Economy, the Federal States of Upper Austria, and Styria as well as the Styrian Business Promotion Agency (SFG). Furthermore, Upper Austrian Research GmbH continuously supports K1-MET. Beside the public funding from COMET, the project is partially financed by the scientific partners acib GmbH, Coventry University, Montanuniversitaet Leoben, University of Natural Resources and Life Sciences, UVR-FIA GmbH, and the industrial partners AUDI AG, BRAIN Biotech AG, Ebner Industrieofenbau GmbH, RHI Magnesita GmbH, Saubermacher Dienstleistungs AG, TÜV SÜD Landesgesellschaft Österreich GmbH, voestalpine High Performance Metals GmbH and VTU Engineering GmbH.

REFERENCES

European Commission. Proposal for a Regulation of the European Parliament and of the Council concerning Batteries and Waste Batteries, Repealing Directive 2006/66/EC and Amending Regulation (EU) 2019/1020: SWD(2020) 334 Final. Available on-line: www.parlament.gv.at/PAKT/ EU/XXVII/EU/04/37/EU_43776/imfname_11029480.pdf

Gerold, E., Lerchbammer, R., Antrekowitsch H. (2022). Parameter study on the recycling of LFP cathode material using hydrometallurgical methods. *Metals*, 12 (10), 1706. https://doi.org/10.3390/met12101706.

Global Battery Alliance. A vision for a sustainable battery value chain in 2030: Unlocking the full potential to power sustainable development and climate change mitigation. In: *World Economic Forum 2019*, pp. 1–52.

Holzer, A., Baldauf M., Wiszniewski, L., Windisch-Kern, S., Raupenstrauch, H. (2022a). Influence of impurities on the high-temperature behavior of the lithium-ion battery cathode material NMC under reducing conditions for use in the Indured reactor concept. *Detritus* (20), 22–28. https://doi.org/10.31025/2611-4135/2022.15215.

Holzer, A., Wiszniewski, L., Windisch-Kern, S., Raupenstrauch, H. (2022b). Optimisation of a pyrometallurgical process to efficiently recover valuable metals from commercially used lithium-ion battery bathode materials LCO, NCA, NMC622, and LFP. *Metals*, 12 (10), 1642. https://doi.org/10.3390/met12101642.

Holzer, A., Zimmermann, J., Wiszniewski, L., Necke, T., Gatschlhofer, C., Öfner, W., Raupenstrauch, H. (2023). A combined hydro-mechanical and pyrometallurgical recycling approach to recover valuable metals from lithium-ion batteries avoiding lithium slagging. *Batteries*, 9 (1), 15. https://doi.org/10.3390/batteries9010015.

Johnston, W. D., Heikes, R. R., Sestrich, D. (1958). The preparation, crystallography, and magnetic properties of the LixCo(1−x)O system. Journal of Physics and Chemistry of Solids 7 (1), 1–13. https://doi.org/10.1016/0022-3697(58)90175-6.

Kim, S., Bang, J., Yoo, J., Shin, Y., Bae, J., Jeong, J., Kim, K., Dong, P., Kwon, K., (2021). A comprehensive review on the pre-treatment process in lithium-ion battery recycling. *Journal of Cleaner Production*, 294, 126329. https://doi.org/10.1016/j.jclepro.2021.126329.

Kwon, O., Sohn, I. (2020). Fundamental thermokinetic study of a sustainable lithium-ion battery pyrometallurgical recycling process. *Resources, Conservation and Recycling*, 158, 104809. https://doi.org/10.1016/j.resconrec.2020.104809.

Lamnatou, C., Chemisana, D., Cristofari, C. (2022). Smart grids and smart technologies in relation to photovoltaics, storage systems, buildings and the environment. Renewable Energy, 185, 1376–

1391. https://doi.org/10.1016/j.renene.2021.11.019.
Liu, J., Wang, H., Hu, T., Bai, X., Wang, S., Xie, W., Hao, J., He, Y., (2020). Recovery of $LiCoO_2$ and graphite from spent lithium-ion batteries by cryogenic grinding and froth flotation. *Minerals Engineering*, 148, 106223. https://doi.org/10.1016/j.mineng.2020.106223.
Natarajan, S., Boricha, A.B., Bajaj, H.C. (2018). Recovery of value-added products from cathode and anode material of spent lithium-ion batteries. *Waste Management*, 77, 455–465. https://doi.org/10.1016/j.wasman.2018.04.032.
Nguyen, T., Schnidrig, J., Maréchal, F. (2021). An analysis of the impacts of green mobility strategies and technologies on different European energy systems. Cost, optimisation, simulation and environmental impact of energy systems. Available online at https://infoscience.epfl.ch/record/288732/files/paper_113.pdf?ln=en.
Nurdiawati, A., Urban, F. (2021). Towards deep decarbonisation of energy-intensive industries: A review of current status, technologies and policies. *Energies*, 14 (9), 1-33. https://doi.org/10.3390/en14092408.
Or, T., Gourley, S.W.D., Kaliyappan, K., Yu, A., Chen, Z. (2020). Recycling of mixed cathode lithium-ion batteries for electric vehicles: Current status and future outlook. *Carbon Energy*, 2 (1), 6–43. https://doi.org/10.1002/cey2.29.
Ponak, C. (2019). Carbo-thermal reduction of basic oxygen furnace slags with simultaneous removal of phosphorus via the gas phase. Dissertation. Leoben, Montanuniversitaet Leoben. Available online at https://pure.unileoben.ac.at/portal/files/4334924/AC15512521n01.pdf (accessed 2/7/2023).
Ruismäki, R., Rinne, T., Dańczak, A., Taskinen, P., Serna-Guerrero, R., Jokilaakso, A. (2020). Integrating flotation and pyrometallurgy for recovering graphite and valuable metals from battery scrap. *Metals*, 10 (5), 680. https://doi.org/10.3390/met10050680.
Sojka, R., Pan, Q., Billman, L. (eds.) (2020). Comparative study of lithium-ion battery recycling processes. Salzburg, *Proceedings of the 25th International Conference on Battery Recycling ICBR 2020*.
Sommerfeld, M., Vonderstein, C., Dertmann, C., Klimko, J., Oráč, D., Miškufová, A., Havlík, T., Friedrich, B. (2020). A combined pyro- and hydrometallurgical approach to recycle pyrolyzed lithium-ion battery back mass Part 1: Production of lithium concentrates in an electric arc furnace. *Metals*, 10 (8), 1069. https://doi.org/10.3390/met10081069.
Teske, S., Pregger, T., Simon, S., Naegler, T., Pagenkopf, J., Deniz, Ö., van den Adel, B., Dooley, K., Meinshausen, M. (2021). It is still possible to achieve the Paris Climate Agreement: Regional, sectoral, and land-use pathways. *Energies*, 14 (8), 2103. https://doi.org/10.3390/en14082103.
Vest, M. (2016). Weiterentwicklung des pyrometallurgischen IME recyclingverfahrens für Li-ionen catterien von elektrofahrzeugen. Ph.D. Thesis, RWTH Aachen, Germany.
Windisch-Kern, S., Holzer, A., Ponak, C., Hochsteiner, T., Raupenstrauch, H. (2021a). Thermal analysis of lithium ion battery cathode materials for the development of a novel pyrometallurgical recycling approach. *Carbon Resources Conversion*, 4, 184–189. https://doi.org/10.1016/j.crcon.2021.04.005.
Windisch-Kern, S., Holzer, A., Wiszniewski, L., Raupenstrauch, H. (2021b). Investigation of potential recovery rates of nickel, manganese, cobalt, and particularly lithium from NMC-type cathode materials ($LiNi_xMn_yCo_zO_2$) by carbo-thermal reduction in an inductively heated carbon bed reactor. *Metals*, 11 (11), 1844. https://doi.org/10.3390/met11111844.
Xu, C., Dai, Q., Gaines, L., Hu, M., Tukker, A., Steubing, B. (2020). Future material demand for automotive lithium-based batteries. *Communications Materials*, 1, 99. https://doi.org/10.1038/s43246-020-00095-x.
Yu, D., Huang, Z., Makuza, B., Guo, X., Tian, Q. (2021). Pre-treatment options for the recycling of spent lithium-ion batteries: A comprehensive review. *Minerals Engineering*, 173, 107218. https://doi.org/10.1016/j.mineng.2021.107218.
Zhang, T., He, Y., Wang, F., Ge, L., Zhu, X., Li, H. (2014). Chemical and process mineralogical characterisations of spent lithium-ion batteries: an approach by multi-analytical techniques. *Waste Management*, 34 (6), 1051–1058. https://doi.org/10.1016/j.wasman.2014.01.002.
Zhao, Y., Pohl, O., Bhatt, A.I., Collis, G.E., Mahon, P.J., Rüther, T., Hollenkamp, A.F. (2021). A review on battery market trends, second-life reuse, and recycling. *Sustainable Chemistry*, 2 (1), 167–205. https://doi.org/10.3390/suschem2010011.